Non-basal dislocations should be accounted for in simulating ice mass flow

T. Chauve[a], M. Montagnat[a], S. Piazolo[b,c], B. Journaux[a], J. Wheeler[d], F. Barou[e], D. Mainprice[e], A. Tommasi[e]

[a] *Univ. Grenoble Alpes, CNRS, IRD, G-INP*[1]*, IGE, F-38000 Grenoble, France*
[b] *ARC Center of Excellence for Core to Crust Fluid Systems (CCFS) and GEMOC, Department of Earth and Planetary Science, Macquarie University, NSW 2109, Australia*
[c] *School of Earth and Environment, University of Leeds, Leeds LS2 9JT, UK*
[d] *Department of Earth and Ocean Sciences, School of Environmental Science, University of Liverpool, Liverpool L69 3GP, UK*
[e] *Geosciences Montpellier, Université de Montpellier / CNRS F-34095 Montpellier, France*

Abstract

Prediction of ice mass flow and associated dynamics is pivotal at a time of climate change. Ice flow is dominantly accommodated by the motion of crystal defects - the dislocations. In the specific case of ice, their observation is not always accessible by means of the classical tools such as X-ray diffraction or transmission electron microscopy (TEM). Part of the dislocation population, the geometrically necessary dislocations (GNDs) can nevertheless be constrained using crystal orientation measurements via electron backscattering diffraction (EBSD) associated with appropriate analyses based on the Nye (1950) approach. The present study uses the Weighted Burgers Vectors, a reduced formulation of the Nye theory that enables the characterization of GNDs. Applied to ice, this method documents, for the first time, the presence of dislocations with non-basal $[c]$ or $< c+a >$ Burgers vectors. These $[c]$ or $< c+a >$ dislocations represent up to 35% of the GNDs observed in laboratory-deformed ice samples. Our findings offer a more complex and comprehensive picture of the key plasticity processes responsible for polycrystalline ice creep and provide better constraints on the constitutive mechanical laws implemented in ice sheet flow models used to predict the response of Earth ice masses to climate change.

Keywords:
Non-basal dislocations in ice, Weighted Burgers Vectors, cryo-EBSD, crystal plasticity

1. Introduction

Understanding the deformation behavior of ice crystals is essential for modeling the flow of glaciers and ice sheets. Ice on Earth, ice Ih, has an hexagonal crystalline structure. It has a strong viscoplastic anisotropy, since deformation occurs almost exclusively by dislocation glide on the basal plane (Duval et al., 1983). This crystal-scale anisotropy results in strong textures (crystallographic orientations) and, hence, in large-scale texture-induced anisotropy. This anisotropy has crucial effects on large-scale ice flow (e.g. Durand et al. (2007)). It is responsible, for instance, for abrupt changes in rheology between the ice sheet and the ice

[1] Institute of Engineering Univ. Grenoble Alpes

shelf (Ma et al., 2010) and for basal folding (Bons et al., 2016). The viscoplastic anisotropy of ice crystals also results in strong strain and stress heterogeneity (Grennerat et al., 2012), leading to dynamic recrystallization (Duval et al., 1983; Chauve et al., 2015), a process that is essentially controlled by the dislocation behavior and interactions (Chauve et al., 2017). Ice is therefore a good analogue to study the behaviour of materials with high viscoplastic anisotropy deforming at high temperature ($T/T_{melt} > 0.9$), such as the Earth lower crust and mantle, where the dominant rock-forming minerals (e.g. feldspar, quartz, olivine, pyroxenes, micas) are highly anisotropic.

However, the difficulty in observing dislocations by TEM or X-ray diffraction results in a lack of knowledge on the activity of other slip systems or of mechanisms such as climb or cross-slip that may complement basal glide. The lack of constraints on the activity of the non-basal slip systems in ice limits the ability of micro-macro crystal plasticity methods to simulate the mechanical behaviour of ice and its evolution (see Montagnat et al. (2014) for a review). To approach a realistic mechanical behaviour, which can be used to model the flow of glaciers and polar ice sheets, strong assumptions have been made (see Castelnau et al. (1997); Kennedy et al. (2013) for instance). In particular, in all models based on crystal plasticity, four to five independent slip systems are required to maintain strain compatibility (Hutchinson, 1977), hence for ice, glide on non-basal slip systems is allowed. Castelnau et al. (1997) imposed a non basal activity 70 times harder than basal activity, while Llorens et al. (2016) lowered this ratio to 20, enabling a significant contribution of non-basal systems to deformation, without any experimental evidence to stand on.

Most observed dislocations in ice so far have one of the three equivalent $1/3 < 2\bar{1}\bar{1}0 >$ Burgers vectors and are constrained to glide in the basal plane (0001) owing to their tendency to dissociate into partial dislocations (Higashi, 1988; Hondoh, 2000). Rare $1/3 < 2\bar{1}\bar{1}0 >$ dislocations have been observed to glide on prismatic planes by X-ray diffraction in low strain conditions where very few dislocations were activated (Shearwood and Withworth, 1989), and when crystals were oriented to minimize the resolved shear stress in the basal plane (Liu and Baker, 1995). Indirect evidence of double cross-slip of basal dislocations was obtained from X-ray diffraction observations on single crystal deformed in torsion (Montagnat et al., 2006). Dislocation Dynamic simulations estimated the local stress necessary to activate this mechanism (Chevy et al., 2012).

So far, direct observations (via X-ray diffraction) of dislocations with Burgers vector $[c] = [0001]$ or $< c + a >= 1/3 < 11\bar{2}3 >$ are limited to very specific conditions such as peripheral dislocations of stacking faults formed during crystal growth or under cooling (Higashi, 1988). The formation of stacking faults under cooling is assumed to result from climb of the basal component of dislocation loops with $< c + a >$ Burgers vector, induced by the precipitation of excess point defects generated by cooling. Dislocation loops with $[c]$-component Burgers vectors were also observed to form due to tiny inclusions (water droplets for pure ice, or solute pockets for NH_3-doped ice) formed during crystallization and due to thermal stress imposed in the crystal growing apparatus (Oguro and Higashi, 1971). To our knowledge, there are no other direct observations of dislocations with a $[c]$-component Burgers vector for pure or natural ice.

Weikusat et al. (2011b) indirectly inferred $[c]$ or $<c+a>$ dislocations as necessary to explain some subgrain boundary structures observed in ice core samples. The techniques used (surface sublimation to extract subgrain boundaries and discrete X-ray Laue diffraction analyses

to obtain local orientations along profiles) did not provide full constraints on the nature of the subgrain boundaries. Nevertheless, by assuming that the subgrain boundaries were perpendicular to the surface, some could be interpreted as tilt boundaries composed of $[c]$ or $< c + a >$ dislocations.

Dislocations are nucleated and contribute to plastic deformation by gliding. The dislocations can be stored in the microstructure by two modes; as trapped dislocations due to dislocation interaction, called Statistically Stored Dislocations (SSDs) and as Geometrically Necessary Dislocations (GNDs) (Fleck et al., 1994). GNDs are intimately associated with lattice curvature, and hence contribute to local strain that can be detected by EBSD as misorientation gradients. They contribute to heterogeneous plastic strain, such as bending or twisting but they can develop even though the experimental conditions allows the possibility of a homogeneous deformation (Van der Giessen and Needleman, 2003). It is generally acknowledged that density of GNDs is significantly higher than density of SSDs (Kubin and Mortensen, 2003).

EBSD analyses of ice were recently made possible thanks to cryo-stages able to maintain samples at very cold temperatures (-100 to -150°C), under low vacuum. This technique gives access to full crystal orientations over reasonably large polycrystalline samples (few cm^2), with a good spatial resolution (down to 0.1 μm). The first applications of EBSD on ice were oriented towards full crystal orientation measurements at the grain level (Obbard et al., 2006). High spatial resolution crystal misorientations within grains were recently used to characterize dislocation substructures (Piazolo et al., 2008; Montagnat et al., 2011; Weikusat et al., 2011a; Montagnat et al., 2015; Chauve et al., 2017). EBSD observations performed in the above mentioned studies are post-mortem and therefore record the effects of the GNDs remaining after relaxation of the internal stress field through anelastic deformation.

Since conventional EBSD maps are 2D, they do not give access to the full dislocation (Nye) tensor $\boldsymbol{\alpha}$ but only to five components $(\alpha_{12}, \alpha_{21}, \alpha_{13}, \alpha_{23}, \alpha_{33})$ where the subscript 3 refers to the normal to the EBSD surface. By this mean, EBSD observations provide lower bounds of GND density (Pantleon, 2008). Recently, Wheeler et al. (2009) proposed a method of characterization of the GNDs called the "weighted Burgers vector" (WBV) (see Appendix A for a detailed description). It corresponds to the projection of the Nye tensor on the EBSD surface and can be expressed as $\boldsymbol{WBV} = (\alpha_{13}, \alpha_{23}, \alpha_{33})$. The WBV tool does not aim at approaching the full dislocation density tensor (as attempted by Pantleon (2008) for instance), but does not require the third dimension to provide meaningful information about the GND population. Its amplitude gives a lower bound for the density of GNDs and its direction refers to the Burgers vector of the sampled GNDs. One important point is that although the WBV does not record all the GNDs present, it cannot contain phantom directions. If it has a significant $[c]$-component then at least some of the Burgers vectors of the GNDs must have a $[c]$-component though this does not mean they have to be parallel to $[c]$.

As for the Nye tensor, the WBV analysis only reflects the GND contribution to the dislocation density. Without further assumptions, this contribution cannot be directly related to the mobile dislocations responsible for most of the plastic deformation.

Cryo-EBSD associated with the WBV analysis was recently shown to be very efficient to characterize the nature of GNDs in ice (Piazolo et al., 2015). Although restricted to small areas, this previous study revealed a contribution of dislocations with $[c]$- or $< c + a >$-component. These observations encouraged us to perform new EBSD observations on ice

polycrystals deformed in the laboratory, with a higher spatial resolution and over larger areas than in the preliminary study of Piazolo et al. (2015).
The present work aims therefore at (i) documenting the presence of dislocations with Burgers vectors comprising a component along $[c]$, (ii) estimating quantitatively the significance of these dislocations within the observed GNDs, and (iii) discussing the implication of this observation for the micro-macro modeling of ice mechanical behaviour, up to the scale of glaciers and polar ice flow.

2. Material and Methods

Large ice polycrystalline samples were deformed in torsion and uniaxial unconfined compression under constant imposed load at high homologous temperature ($T/T_{melt} \sim 0.98$, in a cold room). The samples deformed by compression had a columnar initial grain shape with large grain size (1 to 4 cm^2) (see Grennerat et al. (2012); Chauve et al. (2017) for details) and were deformed under a constant load of 0.5 MPa applied in the plane perpendicular to the column directions, up to a macroscopic strain of about 3%. Torsion tests were performed on solid cylinders (radius $\times$ height $=$ 18 $mm \times 60$ mm) of granular ice (millimetre grain size), under a maximum applied shear stress at the outer radius between 0.5 and 0.6 MPa (experimental conditions similar to the ones in Bouchez and Duval (1982); Montagnat et al. (2006)). Several tests enabled to cover a range of maximum shear strain between 0.01 and 2. These two experimental conditions are complementary. The compression tests enable to follow the first step of deformation in a model microstructure invariant in the third dimension (parallel to the columns) that is close to a 2.5D configuration, where surface observations are a good proxy to the bulk mechanisms (Grennerat et al., 2012). The torsion experiments give access to large strain levels on an initially isotropic microstructure and texture. A summary of the experimental conditions of the tests used in this study is given in table 1.

Id	**Sample**	**Mechanical test**	**T** $°C$	**Stress**	ε_{max}	γ_{max}
CI01	Columnar ice	Uniaxial comp.	-7	0.5 MPa	0.03	
TGI01	Granular ice	Torsion	-7	0.46 MPa	0.006	0.012
TGI02	Granular ice	Torsion	-7	0.49 MPa	0.1	0.2
TGI03	Granular ice	Torsion	-7	0.59 MPa	0.21	0.42
TGI04	Granular ice	Torsion	-7	0.63 MPa	0.87	1.96

Table 1: Summary of the experimental conditions for the tests used in the study. Compression tests were performed under constant applied load, and torsion test under constant applied torque (the corresponding maximum shear stress is given here).

Samples (20×10×3 mm^3) were extracted from the deformed blocks for cryo-EBSD observations (angular resolution of 0.7°, spatial resolution of 5 and 20 μm for this study). The torsion samples were cut perpendicular to the radius, as close as possible to the external side of the cylinder. Appropriate adjustment of the vacuum and temperature (1 Pa and -100°C) to reduce sublimation was made following Montagnat et al. (2015). This allowed EBSD mapping of the entire selected areas with indexation rates higher than 85%.
At the compression and shear strains reached, dynamic recrystallization mechanisms such as nucleation at triple junctions, highly misoriented subgrain boundaries and kink bands are

observed as in Chauve et al. (2017). In the compression sample analyses we focused on grain boundaries and triple junction areas. "Typical" dislocation substructures are presented in figures 1 and 2. Similar features were observed in the torsion samples. In these samples, we analyzed larger areas in order to obtain statistical information about the nature of the dislocations involved in the observed substructures.

In order to characterize the dislocations involved in the formation of subgrain boundaries, we used WBV analyses following Wheeler et al. (2009) (see Appendix A for a detailed description). The WBV represents the sum over different dislocation types of the product of [(density of intersections of dislocation lines within a selected area of the map) $\times$ (Burgers vector)]. Each dislocation line crossing the EBSD surface contributes to the WBV but the weight of this contribution depends of the angle between the dislocation line and the EBSD surface. It is one (zero) if the dislocation line is perpendicular to (within) the EBSD surface. The WBV analysis gives a vector which can be expressed in the crystal or sample reference frame.

The WBV analyses were performed as (i) a point by point analysis that enables to plot the WBV direction and magnitude along the dislocation substructures and (ii) an integral WBV calculation of the net Burgers vector content of dislocations intersecting a given area of a map by an integration around the edge of this area. The integral WBV calculated over a given area is projected over the four non-independent lattice components of the hexagonal symmetry ($[11\bar{2}0]$,$[\bar{2}110]$,$[1\bar{2}10]$ and $[0001]$ noted $WBV_{a1}, WBV_{a2}, WBV_{a3}, WBV_c$). This integral WBV analysis complements the point-by-point WBV calculations and, due to the integration over an area, reduces the noise level in the analysis (see Appendix A). In special cases the integration also induces a loss of information. For instance, in the case of an integral calculation over an area containing a perfect kink band, the resulting integral WBV will be null if the two opposite tilt bands have similar misorientation angles.

The proportion of dislocations with a $[c]$-component Burgers vector (that includes dislocations with $[c]$ and $< c + a >$ Burgers vectors, thereafter referred to as $[c]$-component dislocations) in the subgrain boundaries is estimated as the ratio between the $WBVc$ component over the Euclidian norm of the WBV ($|WBV_c|/||\mathbf{WBV}||$), thereafter called $rWBV_c$. For the pixel-scale calculations, a cut-off value was defined in such a way to restrict the analysis to sub-structures with a misorientation higher than 0.9°, to remain slightly above the EBSD resolution. This cut-off value transposed to the WBV norm depends on the EBSD step-size since the WBV is calculated per unit length (1.4×10^{-3} μm^{-1} for 5 μm EBSD step size and 3.5×10^{-4} μm^{-1} for 20 μm EBSD step size). Subgrain boundaries are distinguished by selecting the pixels for which the norm of the WBV is higher than this threshold and lower that the upper bound for a subgrain boundary set at 7° of misorientation (Chauve et al., 2017). The cut-off value is coherent with the limit of accuracy of EBSD data and leads to a good agreement with the subgrain boundary segmentation defined based on the local misorientation only. By doing so, less that 1% of pixels are selected as "sub-structures" in the non deformed sample and the corresponding values of $|WBV_c|/||\mathbf{WBV}||$ are uniformly distributed.

The WBV analyses are associated with classical measurements of the rotation axis of the misorientation induced by the subgrain boundary (by making use of absolute orientations from EBSD data) together with the orientation of the boundary trace. From this method

known as "boundary trace analysis" (Mainprice et al., 1993; Lloyd et al., 1997; Prior et al., 2002; Piazolo et al., 2008), the boundary plane can be inferred. These information are used as a visualisation tool in figure 2.
Finally, statistical analyses were performed by using a probability density function that represents the ratio between the number of pixels with a WBV norm higher than the threshold (defined above) over the total number of pixels. It can be seen, for instance in figure 4, that this ratio is small for the low torsion strain experiment. The pixels with a WBV norm higher than the threshold are also separated as a function of the nature of the WBV, meaning mostly composed of $[c]$-component dislocations, mostly composed of $< a >$ dislocations, or composed of a similar amount of both types of dislocations.

3. Experimental observations

We present first detailed observations of a few subgrain boundaries that illustrate the techniques used to distinguish $< a >$ from $[c]$-component Burgers vectors on GND substructures, and then a global analysis performed over large-scale EBSD maps containing hundreds of grains (from the torsion test samples), which aims at evaluating the statistical significance of the dislocations with $[c]$-component Burgers vectors within the substructures. Frequently observed subgrain structures in ice deformed by plasticity include "closed" shaped subgrain boundaries (SGBs) formed in the vicinity of serrated grain boundaries (Fig. 1), in areas where the microstructure is very heterogeneous. These "closed" shaped SGBs were shown in (Chauve et al., 2017) to act as precursor of nucleation by strain induced boundary migration (SIBM) and bulging. The superposition of the WBV data (projection of the WBV on the sample plane and relative contribution of $[c]$-component dislocations, $rWBV_c$) to the trace of the SGBs (Fig. 1) highlights the complexity of the dislocation sub-structures and the variability of the contribution of $[c]$-component Burgers vector dislocations (from almost null to almost 1) in the different subgrain boundary segments.
The "closed loop" substructure on the left side of figure 1 has been selected for a detailed characterization (Fig. 2 and Table 2). It can be separated into three domains with distinct WBV orientations. Two of them, domains 1 and 3, have WBV orientations pointing in two opposite $< m >$ ($< 1\bar{1}00 >$) axis directions. These two subgrains accommodate a rotation around an axis parallel to the boundary plane (along $< a >$ axes) but with opposite rotation directions. Such a configuration, characteristic of two tilt-bands with opposite signs, forming a kink band, is frequently observed in ice (Montagnat et al., 2011; Piazolo et al., 2015).
The subgrain boundary in domain 2 is characterized by a boundary plane that is perpendicular to the ones of the SBGs from domains 1 and 3. However its rotation axis is also parallel to an $< a >$ axis and it is contained within the subgrain boundary plane. Subgrain segment 3 is therefore also a tilt boundary. The WBVs are, this time, aligned along the $[c]$ axis and perpendicular to the rotation axis. This configuration cannot be explained without an important contribution of edge dislocations with a $[c]$-component Burgers vectors. This interpretation is confirmed quantitatively by the estimation of the integral WBV in the three areas of interest (table 2). The relative contribution of the $[c]$-component dislocations, which is estimated as the ratio $rWBVc$ is shown to dominate in domain 2.

The torsion experiments provide samples deformed in simple shear in the range $\gamma = 0.012$

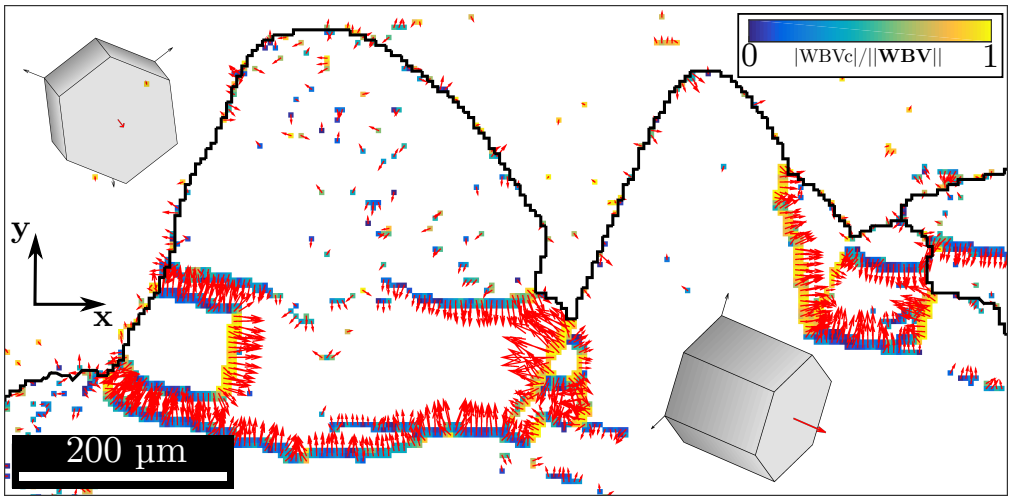

Figure 1: Serrated grain boundary observed in sample CI01. The ratio $\frac{|WBV_c|}{||\mathbf{WBV}||}$ (see text) and the WBVs are plotted for the pixels where $||\mathbf{WBV}||$ is higher than 1.4×10^{-3} μm^{-1}. The red arrows show the in-plane projections of the WBV direction (above a threshold of 1.4×10^{-3} μm^{-1}, EBSD step size 5 μm).

Analyzed area	Integral WBV μm^{-2}				
	WBV_{a1}	WBV_{a2}	WBV_{a3}	WBV_c	$\|WBV_c\|/\|\|\mathbf{WBV}\|\|$
1	−2.77	1.14	1.64	−0.12	0.03
2	−0.60	0.47	0.13	2.65	0.94
3	1.84	−1.02	−0.82	−0.16	0.06

Table 2: Integral WBV projections over the four non-independent axes of the hexagonal crystal symmetry and the ratio $rWBV_c$ (see Materials and Methods), calculated for the areas of sample CI01 selected in figure 2.

to 1.94, for which EBSD observations reveal a high density of subgrain boundaries (Fig. 3). For each sample, the local WBV analysis was performed over the entire mapped surface (about 20×10 mm^2). In figure 3a, data for the most deformed sample are plotted as a function of the relative amount of [c]-component dislocations, $rWBV_c$. This analysis highlights the high frequency of subgrain boundaries with a high proportion of [c]-component dislocations (yellow pixels in figure 3). The [c]-component dislocations are not confined to grain boundary areas, as some subgrain boundaries in the central part of grains display non-negligible contribution of [c]-component dislocations (Fig. 3c).

Similar analyses were performed on samples deformed up to different finite shear strains. The resulting evolution of the relative occurrence of GNDs composed of [c]-component dislocations with finite strain is presented in figure 4. Although the overall number of pixels with a significant WBV magnitude increases significantly with strain, the ratio of substructure composed of [c]-component dislocations remains stable. Except for the almost non-deformed sample, which shows a higher proportion of [c]-component dislocations, about 65% of the pixels belonging to substructures are made of $< a >$ dislocations, whereas the substructures containing [c]-component dislocations represent a non-negligible contribution of about 35% (substructures with clear [c]-component dislocation dominant are 13%, those including similar proportion of $< a >$ and [c]-component dislocations, 22%)

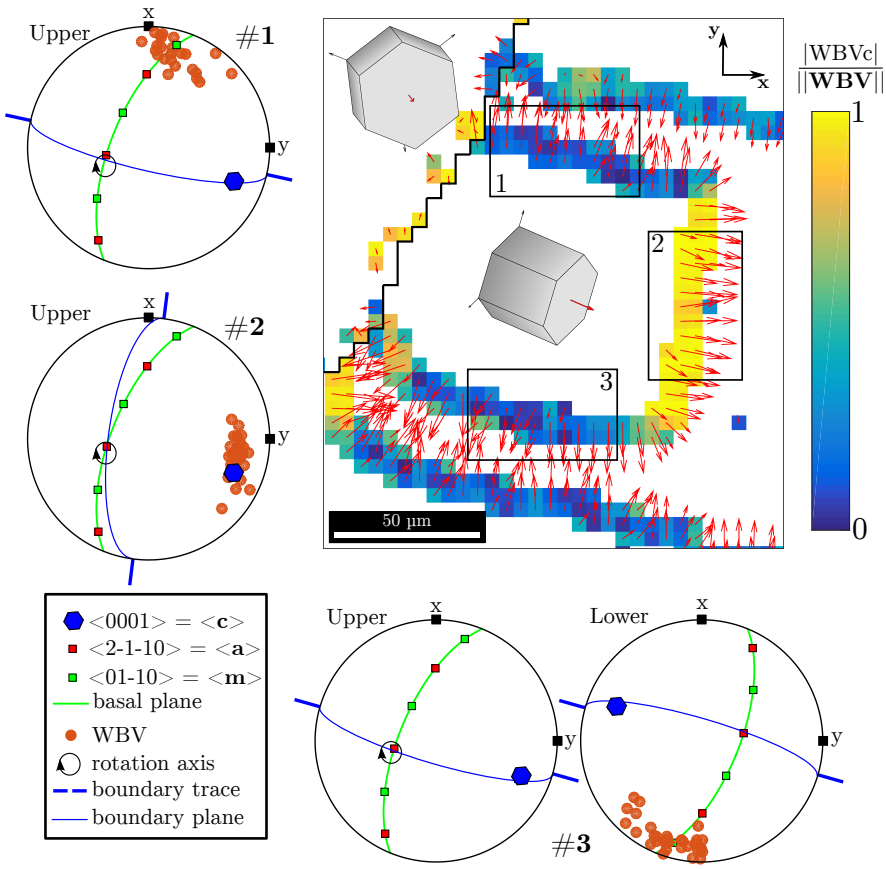

Figure 2: Weighted Burgers Vectors plotted over a zoomed area from the left side of figure 1, sample CI01. The colorscale gives the relative magnitude of [c]-component dislocations, $rWBV_c$, and the red arrows show the in-plane projection of the WBV directions (above a threshold of 1.4×10^{-3} μm^{-1}, EBSD step size of 5 μm). "Boundary plane" refers to "inferred" boundary plane, see text. Rectangular areas mark the domains selected for integral WBV calculations (table 2).

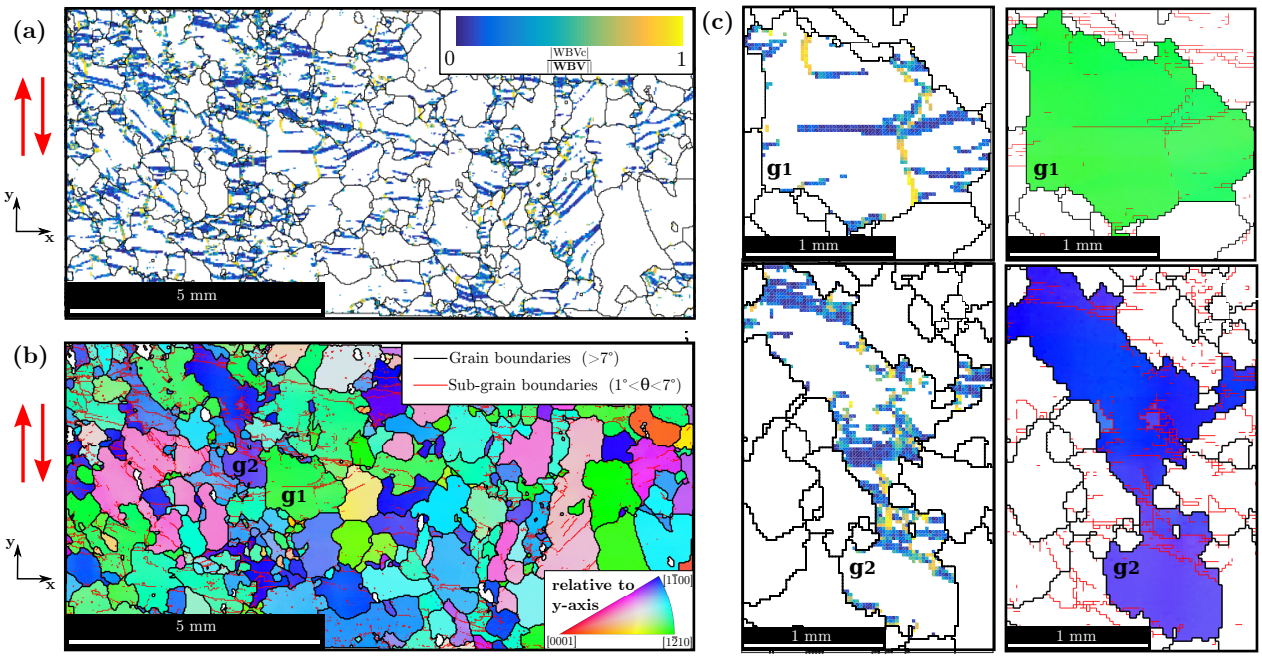

Figure 3: a) Ratio between the $WBVc$ component over the norm of the full WBV ($rWBV_c$) calculated at the pixel scale on sample TGI04 deformed in torsion up to $\gamma = 1.94$. As EBSD step size is 20 μm, a cut-off value of 3.5×10^{-4} μm^{-1} was taken for $||\mathbf{WBV}||$ below which pixels are not considered in the calculation. b) Inverse Pole Figure color-coded EBSD image of the microstructure showing subgrain boundaries (in red) and grain boundaries (in black). c) Four small images to provide a focus on two illustrative cases, with the legend of respectively a) (left) and b) (right).

Another important observation is that at first sight, the presence of dislocations with a $[c]$-

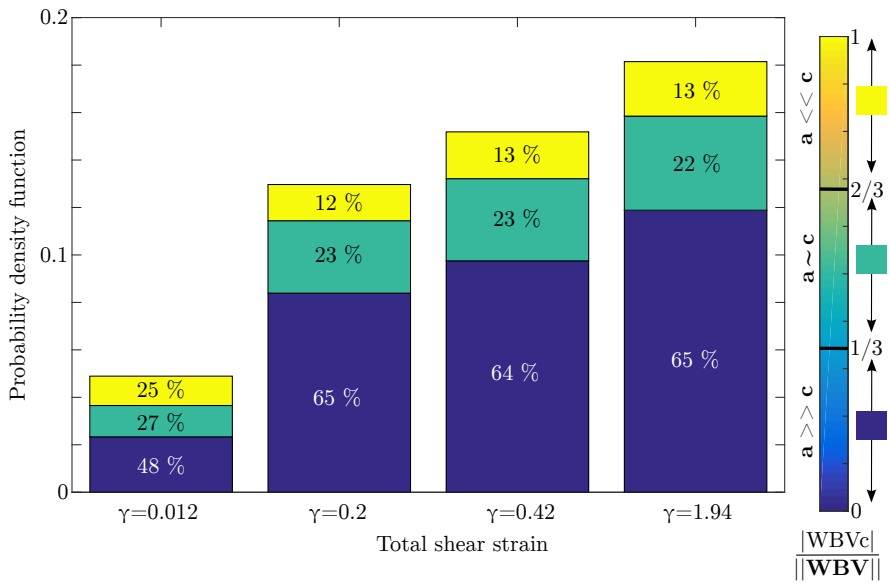

Figure 4: Distribution of pixels with a $||\mathbf{WBV}||$ higher than a threshold of (3.5×10^{-4} μm^{-1}, EBSD step size of 20 μm). Evolution with torsion strain of the relative $[c]$ and $< a >$ components over the norm of the full WBV ($|WBV_c|/||\mathbf{WBV}||$)) for four distinct torsion creep tests.

component Burgers vector does not seem to be correlated with the orientation of the crystal. To further test this point, orientation data at the pixel scale were correlated with the relative amplitude of the WBV components. To do so, we selected data from the sample deformed by torsion at $\gamma = 0.42$ (TGI03), since at this rather low shear strain the macroscopic texture remains reasonably weak to provide a wide enough orientation range (Fig. 5).
As performed in (Grennerat et al., 2012), an adapted Schmid factor, that does not account for slip direction, is used to describe the pixel orientation relative to the imposed stress configuration ($S = \sqrt{|\boldsymbol{\sigma}.\mathbf{c}|^2 - (\mathbf{c}.\boldsymbol{\sigma}.\mathbf{c})^2}$, where $\boldsymbol{\sigma}$ is the stress tensor and $\mathbf{c}$ is the c-axis orientation). The distribution of this Schmid factor (Fig. 5) reveals a slight under representation of orientation with low Schmid factors, which may slightly bias the statistics. With this limitation in mind, figure 5 gives an overview of the relative contributions of the different components of the WBV as a function of the Schmid factor, and therefore as a function of the orientation of the pixel. First, the density of substructures (evaluated by the density of pixels with a WBV norm higher than the threshold) is similar independently of the crystallographic orientation. The slight increase with Schmid factor must result from a statistical bias due to different number of pixels analysed for each orientation range (see top of Fig. 5). Second, dislocations with a $[c]$-component occur within similar proportions for every orientation. This statistical analysis confirms that there is no clear relationship either between local orientation and the density of GNDs, or between local orientation and the type of dislocations involved in the GND substructures.

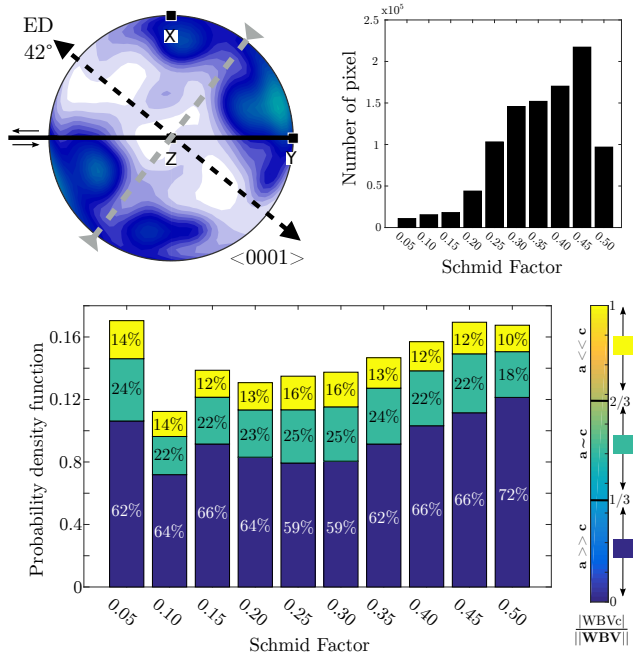

Figure 5: Distribution of the WBV dominant component as a function of the pixel orientation characterised by its adapted Schmid factor ($S = \sqrt{|\boldsymbol{\sigma}.\mathbf{c}|^2 - (\mathbf{c}.\boldsymbol{\sigma}.\mathbf{c})^2}$, where $\boldsymbol{\sigma}$ is the stress tensor and $\mathbf{c}$ is the axis orientation), from the sample TGI03 deformed in torsion up to $\gamma = 0.42$. *Top:* **c**-axis pole figure and distribution of Schmid factors. *Bottom:* Ratio of pixels with $||\mathbf{WBV}||$ higher than 3.5×10^{-4} μm^{-1} (EBSD step size of 20 μm). Each ratio is decomposed in 3 parts showing the dominant component of the WBV.

4. Discussion

From these results, one important observation can be emphasized. Dislocations in ice, more specifically here GNDs, are clearly not composed solely by dislocations with $< a >$ Burgers vectors. A non negligible amount of dislocations with a $[c]$ component in their Burgers vectors contributes to the formation of subgrain boundaries in various configurations (boundary conditions, strain levels...) under laboratory conditions.
Dislocations with a $[c]$ component Burgers vector are theoretically energetically unfavourable, and possess a Peierls barrier up to 10 times the one of $< a >$ dislocations (Hondoh, 2000). They require therefore a higher level of resolved shear stress to be activated. Previous work on ice highlighted the link between local subgrain boundary development and local strain and/or stress concentrations based on misorientation measurements associated with full-field modeling approach (Montagnat et al., 2011; Piazolo et al., 2015), on direct comparison between strain field estimation by Digital Image Correlation and microstructure observations (Chauve et al., 2015) and full-field modeling predictions (Grennerat et al., 2012). Based on these recent works, we can assume that the combined effect of local redistribution of stress due to strain incompatibilities between grains (Duval et al., 1983; Montagnat et al., 2011; Piazolo et al., 2015) and the built up of dislocation fields and their associated internal stress field (Chevy et al., 2012; Richeton et al., 2017) may produce local stresses that allow the activation of non-basal slip systems or the glide of non-basal dislocations, and in particular $[c]$-component dislocations as observed here. The assumed link between local stress concentrations and formation of GNDs is consistent with high-resolution EBSD measurements

recently performed on copper which show a correlation between high GND density and high intragranular residual stresses, directly inferred from HR-EBSD (Jiang et al., 2015).
WBVs only capture part of the GNDs, which are, in turn, a fraction of the total dislocation population. The total contribution of [c]-component dislocations may therefore differ from the present estimations. Moreover, the GNDs populations observed on post-morten 2D cryo-EBSD data might not be proportional to the population of glissile dislocations, that is, representative of the relative activity of the slip systems, which are responsible for deformation. However they are responsible for the accommodation of stress heterogeneities through their contribution to the formation of the subgrain boundaries. By the association of strain measurements by DIC and microstructural observations, Chauve et al. (2015) demonstrated that the formation of subgrain boundaries lead to a marked strain redistribution within a polycrystal, which in the case of kink bands resulted in shear along the newly formed boundaries. GNDs act significantly during dynamic recrystallization by controlling nucleation by SIBM for instance (Piazolo et al., 2015; Chauve et al., 2015). Last but not least, the internal stress fields resulting from dislocation fields (Varadhan et al., 2006) can induce the activation of mechanisms such as climb and cross-slip (Montagnat et al., 2006).. We therefore expect GNDs to play a significant role during deformation at local and large scales.

All micro-macro modelling approaches applied to ice are so far based on drastic assumptions concerning the activated slip systems and on the mechanisms accommodating strain. These assumptions are directly projected on the plasticity (or visco-plasticity) laws describing the dislocation glide and interactions during deformation. In most homogenization approaches (mean or full-field), plasticity is assumed to occur only through dislocation slip on at least four independent slip systems, and their interactions are taken into account by the critical resolved shear stresses which control the relative activities of the various slip systems, and their evolution laws. These laws are generally adjusted based on comparison of the modelled macroscopic mechanical response with experimental results (Castelnau et al., 1996, 2008; Suquet et al., 2012). These assumptions led to an unavoidable minimal activation of non-basal slip which compensates for the lack of knowledge of accommodating mechanisms (climb and cross-slip for instance), and the inability of the models to represent them, except for a few attempts (Lebensohn et al., 2010, 2012). The non-basal activity, and more specifically the fact that a minimum of pyramidal slip-system activity associated with [c] dislocations is always necessary was, until now, not justified by any observations. Most of these empirically adjusted parameters were used in further applications with, sometimes, limited validation tests (Lebensohn et al., 2009; Montagnat et al., 2011; Grennerat et al., 2012; Llorens et al., 2016).
The fact that we have observed for the first time a non-negligible contribution of [c]-component dislocations to the GNDs population in ice polycrystals deformed in the laboratory provides new constraints for modeling the deformation of ice. First, it gives a first order justification for the introduction of the activity of pyramidal slip that requires [c]-component dislocations into crystal plasticity laws. Indeed, Castelnau et al. (2008) and Suquet et al. (2012) both highlighted the necessity of a minimum amount of pyramidal slip to correctly simulate the behavior of ice polycrystals during transient creep by mean of full-field approaches. Secondly, the present observations open the possibility for a direct comparison between model predictions based on Dislocation Dynamics (Devincre et al., 2008) or Dislocation Field approaches

(Taupin et al., 2007, 2008; Richeton et al., 2017) and the actual distribution of $< a >$ and $[c]$-component dislocations in experimentally and naturally deformed ice samples as performed in Richeton et al. (2017). Finally, it suggests the necessity to introduce secondary mechanisms such as climb and cross-slip in the micro-macro approaches just mentioned, that is, of simulating the complexity of dislocation interactions and assessing its impact on the mechanical behaviour.

Only recently attempts have been made to consider the long-range internal stress field associated with dislocation substructures in crystal plasticity models (Taupin et al., 2007, 2008; Richeton et al., 2017). These approaches, based on the elastic theory of continuously distributed dislocations account for the build up of GNDs and their transport during plasticity but they are limited to multi-crystals with few grains (~ 20) because of numerical costs. The validation of these approaches could strongly benefit from an accurate description of the nature of GNDs such as the one presented here. They could, in turn, provide constraints on the internal stress field favorable for the activation of $[c]$-component dislocations.

Coupling detailed analyses of dislocation substructures, like the one presented here, with such models, will produce a new generation of crystal plasticity laws which, when implemented in micro-macro approaches coupled with large-scale flow models, will provide more accurate estimations of the mechanical response of ice in the extreme conditions encountered in natural environments. These large-scale models will be able to accurately represent the texture evolution with strain and, hence, to take into account the mechanical anisotropy associated with the texture evolution with deformation in ice sheets (Gillet-Chaulet et al., 2006). These new plasticity laws will also be able to tackle complex boundary conditions as the cyclic loading encountered in extraterrestrial bodies submitted to tidal forcing, as the saturnian satellite Enceladus (Shoji et al., 2013).

5. Conclusions

The present study reveals for the first time the presence of a non-negligible (between 13% and 35%) proportion of dislocations with $[c]$-component Burgers vector within dislocation substructures in pure ice deformed in the laboratory at close to the melting temperature. The characterization was made possible by the use of Weighted Burgers Vectors (WBV) analyses that estimate the nature of geometrically necessary dislocations (GNDs) from "routine" EBSD measurements. This method is an alternative to classical techniques (X-ray diffraction, TEM) to identify the Burgers vector components of the GNDs, which has proven to be well adapted to the characterization of large, strongly deformed and recrystallized ice samples.

The fraction of dislocations with $[c]$-component Burgers vector in substructures is similar for various strain geometries and levels (compression or torsion creep, low to high strain). As $[c]$-component dislocations are energetically less favourable and possess higher Peierls barriers than $< a >$ dislocations, they are expected in areas submitted to high local stresses. Hence they should play an important role on the dislocation interactions during deformation (responsible for local hardening, internal stress field evolution), but also in the dynamic recrystallization processes (nucleation and grain boundary migration) that strongly impact

microstructure and texture evolution in ice sheets. The present experimental evidence for activation of [c]-component dislocations in ice is a first, but essential step for perfecting the current crystal plasticity models and constraining the simulation of the role of these dislocations on the mechanical response of ice. To be able to represent this complexity in the chain of modeling tools that leads to the prediction of ice sheet and shelf flow is a step further toward an accurate prediction of their evolution in the frame of global climate changes.

6. Acknowledgements

Financial support by the French Agence Nationale de la Recherche is acknowledged (project DREAM, ANR-13-BS09-0001-01). This work benefited from support from institutes INSIS and INSU of CNRS. It has been supported by a grant from Labex OSUG@2020 (ANR10 LABEX56) and from INP-Grenoble and UJF in the frame of proposal called Grenoble Innovation Recherche AGIR (AGI13SMI15). Visiting exchanges for SP and MM were financed by ESF RPN MicroDICE (08RNP003) and by CCFS visiting research funds. MM benefited from a invited researcher fellowship from WSL, at SLF-Davos (2016-2017).

7. References

Bons, P. D., Jansen, D., Mundel, F., Bauer, C. C., Binder, T., Eisen, O., Jessell, M. W., Llorens, M.-G., Steinbach, F., Steinhage, D., Weikusat, I., 2016. Converging flow and anisotropy cause large-scale folding in Greenland's ice sheet. Nat Commun 7.
URL `http://dx.doi.org/10.1038/ncomms11427`

Bouchez, J. L., Duval, P., 1982. The fabric of polycrystalline ice deformed in simple shear : experiments in torsion, natural deformation and geometrical interpretation. Textures and microstructures 5, 171–190.

Castelnau, O., Canova, G. R., Lebensohn, R. A., Duval, P., 1997. Modelling viscoplastic behavior of anisotropic polycrystalline ice with a self-consistent approach. Acta Materialia 45 (11), 4823 – 4834.
URL `http://www.sciencedirect.com/science/article/B6TW8-3SPV0K1-1D/2/4d05120a0c90c52e1e4e3023faba79fb`

Castelnau, O., Duval, P., Montagnat, M., Brenner, R., 2008. Elastoviscoplastic micromechanical modeling of the transient creep of ice. Journal of Geophysical Research Solid Earth 113 (B11203).

Castelnau, O., Thorsteinsson, T., Kipfstuhl, J., Duval, P., Canova, G. R., 1996. Modelling fabric development along the GRIP ice core, central Greenland. Ann. Glaciol. 23, 194–201.

Chauve, T., Montagnat, M., Barou, F., Hidas, K., Tommasi, A., Mainprice, D., 2017. Investigation of nucleation processes during dynamic recrystallization of ice using cryo-EBSD. Phil. Trans. R. Soc. A 375, 20150345.

Chauve, T., Montagnat, M., Vacher, P., 12 2015. Strain field evolution during dynamic recrystallization nucleation; a case study on ice. Acta Materialia 101, 116–124.
URL http://www.sciencedirect.com/science/article/pii/S1359645415006102

Chevy, J., Louchet, F., Duval, P., Fivel, M., 2012. Creep behaviour of ice single crystals loaded in torsion explained by dislocation cross-slip. Phil. Mag. Let. 92 (6), 262–269.

Devincre, B., Hoc, T., Kubin, L., 2008. Dislocation Mean Free Paths and Strain Hardening of Crystals. Science 320 (5884), 1745–1748.
URL http://www.sciencemag.org/cgi/content/abstract/320/5884/1745

Durand, G., Gillet-Chaulet, F., Svensson, A., Gagliardini, O., Kipfstuhl, S., Meyssonnier, J., Parrenin, F., Duval, P., Dahl-Jensen, D., Azuma, N., 2007. Change of the ice rheology with climatic transitions. Implication on ice flow modelling and dating of the EPICA Dome C core. Climates of the Past 3, 155–167.

Duval, P., Ashby, M., Anderman, I., 1983. Rate controlling processes in the creep of polycrystalline ice. J. Phys. Chem. 87 (21), 4066–4074.

Fleck, N., Muller, G., Ashby, M., Hutchinson, J., 1994. Strain gradient plasticity : theory and experiment. Acta Metall. Mater. 42, 475–487.

Gillet-Chaulet, F., Gagliardini, O., Meyssonnier, J., Zwinger, T., Ruokolainen, J., 2006. Flow-induced anisotropy in polar ice and related ice-sheet flow modelling. J. Non-Newtonian Fluid Mech. 134, 33–43.

Grennerat, F., Montagnat, M., Castelnau, O., Vacher, P., Moulinec, H., Suquet, P., Duval, P., 5 2012. Experimental characterization of the intragranular strain field in columnar ice during transient creep. Acta Materialia 60 (8), 3655–3666.
URL http://www.sciencedirect.com/science/article/pii/S1359645412002054

Higashi, A., 1988. Lattice defects in ice crystals. Hokkaido University Press, Sapporo Japan.

Hondoh, T., 2000. Nature and behavior of dislocations in ice. In: Hondoh, T. (Ed.), Physics of Ice Core Records. Sapporo: Hokkaido University Press, pp. 2–34.

Hutchinson, J., 1977. Creep and plasticity of hexagonal polycrystals as related to single crystal slip. Metall. Trans. 8A (9), 1465–1469.

Jiang, J., Benjamin Britton, T., Wilkinson, A. J., 8 2015. Evolution of intragranular stresses and dislocation densities during cyclic deformation of polycrystalline copper. Acta Materialia 94 (0), 193–204.
URL http://www.sciencedirect.com/science/article/pii/S1359645415002736

Kennedy, J. H., Pettit, E. C., L., D. P. C., 2013. The evolution of crystal fabric in ice sheets and its link to climate history. Journal of Glaciology 59 (241), 357–373.

Kubin, L., Mortensen, A., 2003. Geometrically necessary dislocations and strain-gradient plasticity: a few critical issues. Scripta materialia 48 (2), 119–125.

Lebensohn, R. A., Hartley, C. S., Tomé, C. N., Castelnau, O., 02 2010. Modeling the mechanical response of polycrystals deforming by climb and glide. Philosophical Magazine 90 (5), 567–583.
URL http://dx.doi.org/10.1080/14786430903213320

Lebensohn, R. A., Holt, R. A., Caro, A., Alankar, A., Tomé, C. N., 2012. Improved constitutive description of single crystal viscoplastic deformation by dislocation climb. Comptes Rendus Mécanique 340 (4), 289–295.
URL http://www.sciencedirect.com/science/article/pii/S1631072112000484

Lebensohn, R. A., Montagnat, M., Mansuy, P., Duval, P., Meyssonnier, J., Philip, A., 2009. Modeling viscoplastic behavior and heterogeneous intracrystalline deformation of columnar ice polycrystals. Acta Materialia 57 (5), 1405 – 1415.
URL http://www.sciencedirect.com/science/article/B6TW8-4V9252Y-3/2/c091590918643e4f9e7b480ce3cef3f4

Liu, F., Baker, I., 1995. Thermally induced dislocation loops in polycrystalline ice. Phil. Mag. A 71, 1–14.

Llorens, M.-G., Griera, A., Bons, P. D., Lebensohn, R. A., Evans, L. A., Jansen, D., Weikusat, I., 9 2016. Full-field predictions of ice dynamic recrystallisation under simple shear conditions. Earth and Planetary Science Letters 450, 233–242.
URL http://www.sciencedirect.com/science/article/pii/S0012821X16303326

Lloyd, G. E., Farmer, A. B., Mainprice, D., 1997. Misorientation analysis and the formation and orientation of subgrain and grain boundaries. Tectonophysics 279 (1), 55–78.
URL http://www.sciencedirect.com/science/article/pii/S0040195197001157

Ma, Y., Gagliardini, O., Ritz, C., Gillet-Chaulet, F., Durand, G., Montagnat, M., 2010. Enhancement factors for grounded ice and ice shelves inferred from an anisotropic ice-flow model. Journal of Glaciology 56 (199), 805–812.

Mainprice, D., Lloyd, G. E., Casey, M., 1993. Individual orientation measurements in quartz polycrystals: advantages and limitations for texture and petrophysical property determinations. Journal of Structural Geology 15 (9), 1169–1187.
URL http://www.sciencedirect.com/science/article/pii/0191814193901624

Montagnat, M., Blackford, J. R., Piazolo, S., Arnaud, L., Lebensohn, R. A., 2011. Measurements and full-field predictions of deformation heterogeneities in ice. Earth and Planetary Science Letters 305 (1-2), 153 – 160.
URL http://www.sciencedirect.com/science/article/B6V61-52G1S1V-3/2/9c22100ee12109d27e843354e8caa75b

Montagnat, M., Castelnau, O., Bons, P. D., Faria, S. H., Gagliardini, O., Gillet-Chaulet, F., Grennerat, F., Griera, A., Lebensohn, R. A., Moulinec, H., Roessiger, J., Suquet, P., 4 2014. Multiscale modeling of ice deformation behavior. Journal of Structural Geology 61 (0), 78–108.
URL http://www.sciencedirect.com/science/article/pii/S0191814113000837

Montagnat, M., Chauve, T., Barou, F., Tommasi, A., Beausir, B., Fressengeas, C., 2015. Analysis of dynamic recrystallization of ice from EBSD orientation mapping. Frontiers in Earth Science 3 (81).
URL http://www.frontiersin.org/cryospheric_sciences/10.3389/feart.2015.00081/abstract

Montagnat, M., Weiss, J., Chevy, J., Duval, P., Brunjail, H., Bastie, P., Gil Sevillano, J., 2006. The heterogeneous nature of slip in ice single crystals deformed under torsion. Philosophical Magazine 86 (27), 4259–4270.

Obbard, R., Baker, I., Sieg, K., 2006. Using electron backscatter diffraction patterns to examine recrystallization in polar ice sheets. Journal of Glaciology 52 (179), 546–557.

Oguro, M., Higashi, A., 09 1971. Concentric dislocation loops with [0001] Burgers vectors in ice single crystals doped with NH_3. Philosophical Magazine 24 (189), 713–718.
URL http://dx.doi.org/10.1080/14786437108217043

Pantleon, W., 2008. Resolving the geometrically necessary dislocation content by conventional electron backscattering diffraction. Scripta Materialia 58 (11), 994 – 997.
URL http://www.sciencedirect.com/science/article/pii/S1359646208000912

Piazolo, S., Montagnat, M., Blackford, J. R., 2008. Sub-structure characterization of experimentally and naturally deformed ice using cryo-EBSD. Journal of Microscopy 230 (3), 509–519.

Piazolo, S., Montagnat, M., Grennerat, F., Moulinec, H., Wheeler, J., 5 2015. Effect of local stress heterogeneities on dislocation fields: Examples from transient creep in polycrystalline ice. Acta Materialia 90 (0), 303–309.
URL http://www.sciencedirect.com/science/article/pii/S1359645415001615

Prior, D. J., Wheeler, J., Peruzzo, L., Spiess, R., Storey, C., 2002. Some garnet microstructures: an illustration of the potential of orientation maps and misorientation analysis in microstructural studies. Journal of Structural Geology 24 (6-7), 999 – 1011, micro structural Processes: A Special Issue in Honor of the Career Contributions of R.H. Vernon.
URL http://www.sciencedirect.com/science/article/B6V9D-458WFD3-2/2/3cb45b2c164c23c3fdae838da879e0e2

Richeton, T., Le, L., Chauve, T., Bernacki, M., Berbenni, S., Montagnat, M., 2017. Modelling the transport of geometrically necessary dislocations on slip systems: application to single- and multi-crystals of ice. Modelling and Simulation in Materials Science and Engineering 25 (2), 025010.
URL http://stacks.iop.org/0965-0393/25/i=2/a=025010

Shearwood, C., Withworth, R., 1989. X-ray topographic observations of edge dislocation glide on non-basal planes in ice. J.Glaciol. 35 (120), 281–283.

Shoji, D., Hussmann, H., Kurita, K., Sohl, F., 2013. Ice rheology and tidal heating of Enceladus. Icarus 226 (1), 10 – 19.
URL http://www.sciencedirect.com/science/article/pii/S0019103513002042

Suquet, P., Moulinec, H., Castelnau, O., Montagnat, M., Lahellec, N., Grennerat, F., Duval, P., Brenner, R., 2012. Multi-scale modeling of the mechanical behavior of polycrystalline ice under transient creep. Procedia IUTAM 3, 76–90.
URL http://www.sciencedirect.com/science/article/pii/S2210983812000077

Taupin, V., Richeton, T., Chevy, J., Fressengeas, C., Weiss, J., Louchet, F., Miguel, M., 2008. Rearrangement of dislocation structures in the aging of ice single crystals. Acta Materialia 56 (7), 1555 – 1563.
URL http://www.sciencedirect.com/science/article/B6TW8-4RR217B-1/2/5689f7454a1fb98e258daa4f24dcd1df

Taupin, V., Varadhan, S., Chevy, J., Fressengeas, C., Beaudoin, A. J., Montagnat, M., Duval, P., Oct 2007. Effects of size on the dynamics of dislocations in ice single crystals. Phys. Rev. Lett. 99 (15), 155507.

Van der Giessen, E., Needleman, A., 2003. GNDs in nonlocal plasticity theories: lessons from discrete dislocation simulations. Scripta materialia 48 (2), 127–132.

Varadhan, S., Beaudoin, A., Fressengeas, C., 2006. Coupling the dynamic of statistically distributed and excess dislocations. Proc. of Science SMPRI2005, 004, 1–11.

Weikusat, I., De Winter, D. A. M., Pennock, G. M., Hayles, M., Schneijdenberg, C. T. W. M., Drury, M. R., 2011a. Cryogenic EBSD on ice: preserving a stable surface in a low pressure SEM. Journal of Microscopy 242 (3), 295–310.
URL http://dx.doi.org/10.1111/j.1365-2818.2010.03471.x

Weikusat, I., Miyamoto, A., Faria, S. H., Kipfstuhl, S., Azuma, N., Hondoh, T., 2011b. Subgrain boundaries in Antarctic ice quantified by X-ray Laue diffraction. Journal of Glaciology 57 (57), 111–120.

Wheeler, J., Mariani, E., Piazolo, S., Prior, D. J., Trimby, P., Drury, M. R., 2009. The weighted Burgers vector: a new quantity for constraining dislocation densities and types using electron backscatter diffraction on 2D sections through crystalline materials. Journal of Microscopy 233 (3), 482–494.
URL http://dx.doi.org/10.1111/j.1365-2818.2009.03136.x

Appendix A. The Weighted Burgers Vector tool

Dislocations produce local distortions in crystal lattices. When dislocations of different signs are close together these distortions balance out and are not visible at the scale of microns. However when significant numbers of dislocations with the same signs are present, optically visible and (with EBSD) measurable variations of lattice orientation are a consequence the dislocations are then called geometrically necessary dislocations (GNDs). Crystalline materials generally have large elastic moduli meaning that lattice bending due to elastic stress is likely to be small; significant curvature generally relates to the presence of GNDs. Nye (1953) recognized that the lattice curvature can be described by a second rank tensor (now

named after him), in general non-symmetric so having 9 independent components, and that this can be directly linked to the densities of GNDs and their line vectors.

$$\alpha_{i\gamma} = \sum_N \rho^N b_i^N l_\gamma^N \tag{A.1}$$

where (N) indicates the Nth type of dislocation line, and for each type ρ is the density (m^{-2}), b_i the Burgers vector in crystal coordinates (m) and l_γ the unit line vector in sample coordinates. As written the first index in α relates to the crystal reference frame and the second to sample reference frame and its units are m^{-1}.

The idea is explained concisely in (Sutton and Balluffi, 1995). It provides in principle a powerful way of constraining possible GND types from lattice curvature, although there is not a unique way of deciding on dislocation types (lines and Burgers vectors) without further information or assumptions. Using EBSD data from 2D maps only 3 out of the 9 components of the tensor can be unambiguously determined without further assumptions, but Wheeler et al. (2009) argued that even these three can provide valuable insights into possible dislocation types. Specifically the 3 components α_{i3} (where 3 indicates the sample coordinate direction perpendicular to the map) make up a vector related to the Burgers vectors of dislocations present. It is weighted with regard to the individual dislocation densities (through ρ) and the angles the dislocation lines make to the EBSD map (through l_3): hence Weighted Burgers Vector (WBV). For hexagonal phases such as ice the WBV can indicate the presence of vectors with a $[c]$ component. Although the WBV does not record all the GNDs present, it cannot contain phantom directions. If it has a significant $[c]$ component then at least some of the Burgers vectors of the GNDs must have a $[c]$ component though this does not mean they have to be parallel to $[c]$. Wheeler et al. (2009) give two versions of the calculation.

1. In the differential form, local orientation gradients are used to calculate the WBV. Errors are likely to be significant because of error-prone small misorientations, although Wheeler et al. (2009) show how they may be mitigated by filtering out the shortest WBVs. Adjacent measurement points with misorientations above a threshold value are omitted from gradient calculations, so as to exclude high angle boundaries which lack organised dislocation substructures. The magnitude and direction of the WBV can be displayed on maps in a variety of ways. Given that the shortest WBVs are the most error prone, the display may be chosen to show only those above a particular magnitude (cf. Fig 3a).
2. In the integral form, contour integration round the edge of a region on an EBSD map gives the net dislocation content of that region, though the spatial distribution of dislocations (domains of high or low density) within the region are not constrained. The advantage is that errors are lower. This was asserted in (Wheeler et al., 2009) on the basis that numerical integration reduces the effects of noise, and has since been demonstrated using model EBSD maps for distorted lattices with added noise. The method rejects any regions with high angle boundaries intersecting the border, using the threshold value mentioned above. The integral and differential methods are complementary and are built on the same mathematical foundation (they are linked via Stokes theorem).

In this contribution we discuss subgrain boundaries (SGBs). As happens in many materials, GNDs have moved by recovery into discrete structures. As these are two dimensional features, with zero volume, then strictly the dislocation density is infinite. However the integral method still gives a rigorous measure of the dislocation content within a region, if that region includes a subgrain boundary: Sutton and Balluffi (1995) show how closely the analysis of SGBs relates to the analysis of smoothly curved lattices. Hence the direction of the integral WBV still carries useful information related to the GNDs in SGBs. We show colour coded maps of the magnitude of the differential form of the WBV. When this is calculated, numerical differentiation is used. Suppose we have two measurement points with 2.5° difference in orientation separated by a 5 μm step size, then the calculated orientation gradient will be 0.5° / μm. This may in reality be a smoothly curved lattice, or relate to a sharp 2.5° SGB passing between the two measurement points the method cannot distinguish such possibilities. If it is an SGB then a smaller step size of 2.5 μm would give rise to an apparent gradient of 1° / μm. Consequently around SGBs the magnitude of the WBV depends on step size (and hence should be interpreted with caution) but the direction can still be used to constrain GND types.

The disadvantages of the WBV approach are: it is less precise than calculations using high (angular) resolution EBSD (Wallis et al. 2016), it is biased towards dislocation lines intersecting the EBSD map at a high angle, and it does not give a decomposition of the GND population into different dislocation types. The latter can be attempted by making particular assumptions about the dislocation types present and then making a calculation assuming total dislocation energy is minimised. As argued in Wheeler et al. (2009), though, minimising energy without taking into account elastic interactions between dislocations (which will mean that line energies are not simply additive) may not be an appropriate procedure.

The advantages of the WBV are: it can be calculated from routinely collected EBSD data, in a way free from assumptions except that the elastic strains be small. The integral form reduces the propagation of errors inherent in Kikuchi pattern indexing, and can be used to analyse both smoothly curved lattices and SGBs, without any assumptions about twist or tilt nature. As this contribution shows the WBV approach is sufficient to test the hypothesis that dislocations with $[c]$ component Burgers vectors in ice form a significant part of the dislocation substructures.

References - Appendix

Nye, J., 1953. Some geometrical relations in dislocated crystals. Acta Materialia 1, 153162.

Sutton, A. P., Balluffi, R. W., 1995. Interfaces in crystalline materials. Clarendon Press.

Wheeler, J., Mariani, E., Piazolo, S., Prior, D. J., Trimby, P., Drury, M. R., 2009. The weighted Burgers vector: a new quantity for constraining dislocation densities and types using electron backscatter diffraction on 2D sections through crystalline materials. Journal of Microscopy 233 (3), 482494.

Wallis, D., Hansen, L. N., Britton, T. B., Wilkinson, A. J., 2016. Geometrically necessary dislocation densities in olivine obtained using high-angular resolution electron backscatter diffraction. Ultramicroscopy 168, 3445.